Optothermoelectric assembly of plasmonic nanoparticles

A Thesis

submitted to

Indian Institute of Science Education and Research Pune
in partial fulfillment of the requirements for the
BS-MS Dual Degree Programme

by

Utkarsh Khandelwal

Indian Institute of Science Education and Research Pune
Dr. Homi Bhabha Road,
Pashan, Pune 411008, INDIA.

May, 2021

Supervisor: Dr. G.V. Pavan Kumar
© Utkarsh Khandelwal 2021

Certificate

This is to certify that this dissertation entitled Optothermoelectric assembly of plasmonic nanoparticles towards the partial fulfilment of the BS-MS dual degree programme at the Indian Institute of Science Education and Research, Pune represents study/work carried out by Utkarsh Khandelwal at Indian Institute of Science Education and Research under the supervision of Dr. G.V. Pavan Kumar, Associate Professor, Department of Physics , during the academic year 2020-2021.

Dr. G.V. Pavan Kumar

Committee:

Dr. G.V. Pavan Kumar

Dr. Apratim Chatterji

This thesis is dedicated to my family.

Declaration

I hereby declare that the matter embodied in the report entitled Optothermoelectric assembly of plasmonic nanoparticles   are the results of the work carried out by me at the Department of Physics, Indian Institute of Science Education and Research, Pune, under the supervision of Dr. G.V. Pavan Kumar and the same has not been submitted elsewhere for any other degree.

Utkarsh Khandelwal

Acknowledgments

First and foremost, I would like to thank my thesis supervisor Dr. G.V. Pavan Kumar, for his invaluable support and guidance throughout this project. He encouraged me to delve beyond the conventional subject boundaries. Working with him imbibed resilience and persistence in me when looking for innovative solutions for the problem at hand. He encouraged me to delve beyond the conventional subject boundaries. Most importantly, I learned that the best way to understand and work on a problem is by making mistakes, learning, and improvising on them.

Words are not enough to thank my colleagues Surya, Chetna, Dipta, Vandana, Sunny, Shailendra and Rahul. All of them were very helpful and kept the lab atmosphere very friendly. I thank them for being always there when I was stuck and helping me out with their immense knowledge and vast experience. I am incredibly thankful to Sunny, from whom I have learnt quite a bit of everything.

Special thanks to my seniors Vaibhav, Sharvari, Harsh, Rahul and Pavana for taking time out of their busy schedules for me. Sharvari and Harsh were there to listen and answer even the most trivial things. I am highly indebted to them.

Finally, I would like to thank my friends and family for their encouragement and support throughout my studies. It would not have been possible without them.

x

Abstract

Reversible agglomeration of plasmonic nanoparticles has a plethora of applications in material science, nanophotonics and life sciences. Very high power density requirement and increased temperature of trapped metal particle make conventional optical tweezers operating in the visible regime an unfavourable choice to achieve reversible plasmonic aggregate. In this thesis, we elaborately study another mechanism, optothermoelectric trapping, with which metal particles can be reversibly aggregated at very low optical power. It relies on the differential movement of ions in a thermal gradient that arises due to the plasmonic heating of a metal nanostructure when illuminated by light. In the thesis, we first discuss preliminaries, chemical synthesis methods and experimental techniques to setup an optothermoelectric trap. Next, through systematic experimentation and analysis, we study the effect of surfactant concentration, power density, and the excitation wavelength on the metal nanoparticle aggregate. We explore the possibility of in-situ surface-enhanced Raman scattering (SERS) with this assembly. This study has laid down the foundation for multiple future research directions. There is an effort towards creating optothermoelectric trap using a single metal nanoparticle. We are also trying to push the limit of in-situ SERS up to the single-molecule level with the plasmonic aggregate.

Contents

List of Figures

2

List of Tables

Chapter 1

Introduction

It is fascinating how complex behaviour can arise in soft matter systems in ways that are difficult to predict directly from their fundamental constituents. Emergent behaviours, such as self-assembly of colloidal particles, arise due to the subtle interplay of microstructural units, relatively weak interactions, and thermal fluctuations. There has been a tremendous effort to engineer and utilize these interactions so that they organize themselves into a target structure without external intervention. One of the methods to trap micron-sized dielectric particle is by using optical tweezers[9]. It can apply and measure pico-Newton sized forces on such objects under a microscope using a tightly focused light beam. However, the trapping capability of metallic colloids using such an arrangement gets ineffective due to the strong scattering and heating of such metal nanostructures due to localized surface plasmon resonance. Lin et al. have demonstrated a novel approach [8] to manipulate metal nanoparticles of a wide range of materials, sizes and shapes with a single-particle resolution by using a light-directed thermoelectric field that is generated due to spatial separation of dissolved surfactant ions within the heating laser spot. This strategy, called optothermoelectric trapping, allows us to capture and manipulate metal nanoparticles at the single-particle resolution, using a dark field optical imaging setup. Furthermore, it is also possible to create large-scale assemblies of plasmonic nanostructures, which have multiple applications due to the high electric field enhancement in their neighbourhood.

The following sections in this chapter outline the preliminaries necessary to understand the ideas discussed in this thesis. We conclude this chapter by motivating the thesis problem

and defining the structure of this thesis.

1.1 Localised Surface Plasmon Resonance

Plasmons are the quanta of the collective oscillation of free electrons in metals. A *localised surface plasmon* refers to the normal mode of collective oscillation of free electrons confined to a metal nanoparticle. When the laser frequency matches the plasmon frequency of the metal nanoparticle, the resonance condition is reached, and it is called Localised Surface Plasmon Resonance (LSPR).

1.1.1 Metal nanoparticle in static electric field
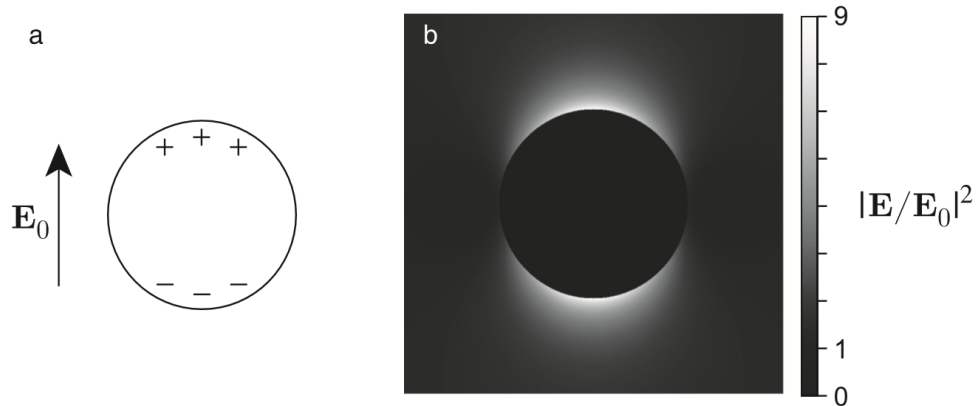
Figure 1.1: a) A metal sphere placed in an electric field b) Local field enhancement near the metal sphere[1]

Consider a metal nanoparticle of radius a in a medium of refractive index $n_s = \sqrt{\varepsilon_s}$. Also, consider the static electric field present in the region as

$$\mathbf{E}_0(\mathbf{r}) = E_0\hat{\mathbf{u}} \quad \text{where} \quad \hat{\mathbf{u}} \text{ is the unit vector along the direction of the electric field.}$$

This electric field displaces the electrons from the equilibrium. A dipole moment is induced due to the charge accumulation. The electric potential in this situation is given by-

$$\phi(r,\theta) = E_0 \left(r - \frac{a^3}{r^2} \right) \cos\theta \tag{1.1}$$

Using this expression, the electric field can be calculated at any point in the space. In particular, at the surface of the metal nanoparticle, the electric field is three times larger than the incident electric field.

$$E_{\text{max}} = 3E_0 \tag{1.2}$$

Now, we know that the enhanced field intensity goes as the square of the enhanced electric field. Therefore, the enhanced field intensity is 9 times as large as the incident field intensity. This substantial near-field enhancement is independent of material properties like refractive index and volume. It is a characteristic of the metal nanoparticle, and this occurs even without plasmon resonance. However, at plasmon resonance, the enhancement crosses this threshold value of 9.

1.1.2   Metal nanoparticle under illumination
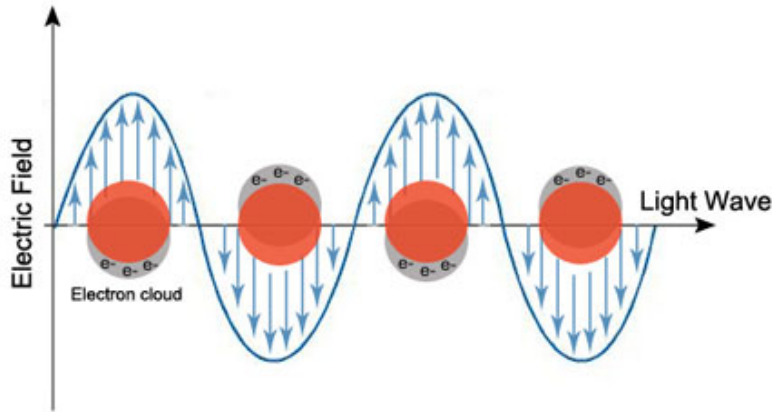
Figure 1.2: A metal sphere placed in a time-harmonic electric field[2]

In time-harmonic electric fields, electrons in the nanostructure oscillate, as shown in figure 1.2. The localised plasmon resonance occurs at a particular frequency ω, which for most noble metals, lies within the visible range. The optical extinction peak is often called localised surface plasmon frequency. The plasmon peak depends on particle composition, size, shape

and refractive index of the surrounding environment. The electric field enhancement factors outside and inside the metal nanoparticle are given by-

$$\eta_{\text{out}} = \frac{E_{\text{out}}}{E_0} = 9 \left| \frac{\varepsilon}{\varepsilon + 2} \right|^2 \tag{1.3}$$

$$\eta_{\text{in}} = \frac{E_{\text{in}}}{E_0} = 9 \left| \frac{1}{\varepsilon + 2} \right|^2 \tag{1.4}$$

It is to be noted that ε for metal is complex quantity, with a negative value of their real part. Therefore, η can be greater than unity. The η values are significant, particularly at the plasmon resonance peak, for two reasons. First, they report the enhancement of electric field in the vicinity of the metal nanoparticle. Second and more importantly, they are unique dimensionless constants for a given metal. For instance, for gold illuminated in vacuum at the plasmon resonance peak of $\lambda = 526$ nm, the value of η_{out} is 19. This enhancement is significantly greater than one observed with the static electric field.

1.2 Heat generation with metal nanoparticles

Metal nanoparticles get strongly heated in the presence of electromagnetic radiation under plasmon resonance. When light interacts with metal, the free electrons start oscillating. This electronic oscillation gives rise to an electronic current and results in energy dissipation via the Joule effect. The heat power density, q is given as-

$$q(\mathbf{r}) = \frac{\omega}{2} \varepsilon_0 \, \text{Im}(\varepsilon) |\mathbf{E}(\mathbf{r})|^2 \tag{1.5}$$

where ω is the angular frequency of excitation and $\mathbf{E}(\mathbf{r})$ is the electric field inside the nanoparticle. The total heat Q generated by the nanoparticle is the integral of $q(\mathbf{r})$ over the entire volume.

$$Q = \frac{\omega}{2} \varepsilon_0 \, \text{Im}\left(\varepsilon_\omega\right) \int_{\text{Vol}} |\mathbf{E}_\omega|^2 \, d\mathbf{r} \tag{1.6}$$

If the radius of the nanoparticle is much smaller than the wavelength of light, then the total heat generate (Q) is given as

$$Q = \frac{\omega}{8\pi} E_\text{o}^2 \left| \frac{3\varepsilon_\text{o}}{2\varepsilon_\text{o} + \varepsilon_{NP}} \right|^2 \text{Im}\,\varepsilon_{NP} \tag{1.7}$$

In presence of multiple nanoparticles, heating effects can be enhanced. This is mainly due
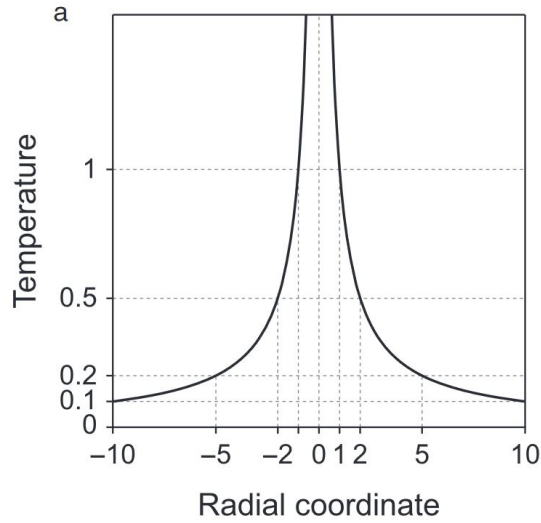
Figure 1.3: Temperature profile in the vicinity of point sized metal heat source. [3]

to two effects[10]-

- **Accumulative effect**- Heat fluxes by multiple nanoparticles are added and there is a larger increase in temperature of the system.

- **Coulomb interaction**- The interaction between multiple nanoparticles is via plasmon-enhanced electric fields. Therefore, the electronic oscillation in a given nanoparticle will be affected due to the electric field created by other nanoparticle. Thus, the resultant net heat generation is dependent on the inter-particle distance and on their arrangement, and can both be enhanced or reduced, depending on the system.

1.3 Optical trapping

The idea of accelerating and trapping particles using light appeared in the 1970 seminal paper of Arthur Ashkin on radiation pressure [11].Optical traps [9]and optical tweezers are uncomplicated yet powerful force probes which has a plethora of applications, particularly in biology. People have been able to perform cell level studies[12], single molecule studies in bacteria [13] and organelle manipulation [14]. Several variations of the optical trap are routinely applied to study the accumulation and dynamics of soft matter [15].

1.3.1 Mechanism

To set up an optical trap, we need a laser beam focused by a high numerical aperture objective lens. Let us consider a spherical dielectric bead of radius a ($a << \lambda$, dipole approximation is valid). An electric dipole moment is induced in such bead when it is placed in the vicinity of a focused laser beam. Due to this induced dipole moment, the entity becomes susceptible to the time-harmonic electric field of light, and thus experiences two competing forces in an optical trap-

- A **gradient force** that pulls the bead towards the center of the focused laser beam. Potential energy of the bead in an optical trap is-

$$U = -\frac{1}{2}\mu.E \ = -\frac{1}{2}\alpha I \ (\because \mu = \alpha E), \tag{1.8}$$

  where α, E and I are the polarizability, electric field and intensity respectively

$$\text{Now, } F_{\text{grad}} = -\nabla U$$

$$\therefore \boxed{F_{\text{grad}} = \frac{1}{2}\alpha\nabla I} \tag{1.9}$$

  Gradient force tends to push the particle towards the most intense part of the laser beam. It depends on the polarizability of the material and the intensity profile of the incident beam. For a loosely focused Gaussian beam, gradient force is unable to trap the particle. However, for a tightly focused Gaussian beam the bead is pushed towards the the beam centre, and there exists a possibility of stable trapping if the gradient force dominates the scattering force.

- A **scattering force** that pushes the bead in the direction of propagation of light. This force arises due to the transfer of momentum from the incident photons to the bead. For bead (radius a),

$$\boxed{F_{\text{scatt}} = \frac{In_m}{c}\frac{128\pi^5 a^6}{3\lambda^4}\left(\frac{m^2-1}{m^2+2}\right)^2} \tag{1.10}$$

  where n_m and m are the refractive indices of the medium and the bead, respectively.

  For a trapped particle, the effect of F_{scat} is to move the bead away from the focus.

Balancing the two forces

$$\text{Now, } F_{\text{grad}} \propto \nabla E^2 r^3$$

$$\text{And, } F_{\text{scatt}} \propto E^2 r^6$$

In most cases, the scattering force dominates over the gradient force. However, when light is focused by a higher numerical aperture objective lens, the focal spot size reduces, and the gradient in the intensity increases. As a result, the gradient force increases significantly, pushing the particle towards the focal point. If the NA is chosen appropriately, the gradient force dominates, and the particle is trapped slightly off the focal point.
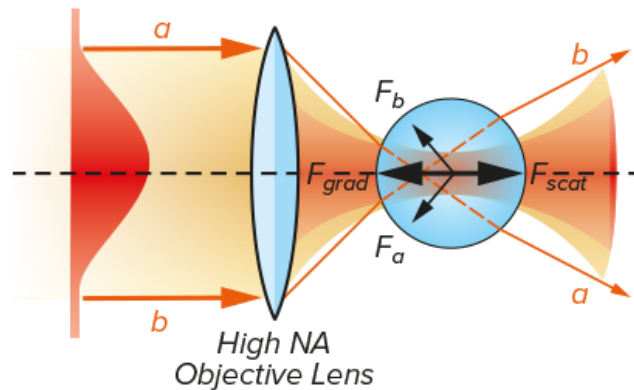
Figure 1.4: Scattering and gradient forces experienced by a dielectric particle in a single beam optical trap balance each other and deem the particle trapped. [4]

Note   When the bead is large (radius $a \gg \lambda$, one can no longer classify the forces as gradient force and scattering force. Trapping, however, is still possible and can be explained in terms of the conservation of linear momentum.

1.4   Thermophoretic trapping

Nanoparticles when dispersed in water exhibit a random motion called Brownian motion. Diffusion coefficient (D) quantifies the rate at which a Brownian particle explores its sur-

roundings.

$$\langle \Delta \mathbf{r}(t)^2 \rangle = 2dDt \tag{1.11}$$

where $\langle \Delta \mathbf{r}(t)^2 \rangle$ is the mean squared displacement of the Brownian particle with diffusion coefficient D exploring d dimensions in time t.

In the presence of a thermal gradient, these particles show a steady drift on top of their random motion. This drift may take the particle away from the heat source or towards it. The drift velocity (v_T) is given by,

$$v_T = -D_T \nabla T \tag{1.12}$$

D_T is the thermal diffusion coefficient of the particle. This phenomenon is known as thermophoresis. It is also called as Ludwig-Soret Effect. It has origins in the reaction force that particle experiences due to the movement of solvent at the particle-solvent boundary layer. Now, to explore the phenomenon in detail, let's consider a nanoparticle with $D_T > 0$.
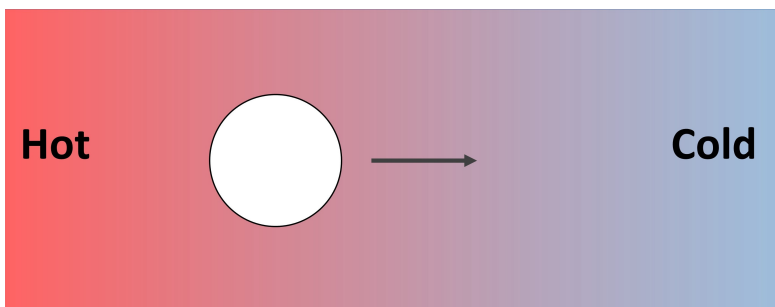
Figure 1.5: A dielectric bead with a positive Soret coefficient in a thermal gradient moves from hot region to cold region.

In this case, the particle will tend to move opposite to the heat gradient. As a result, particle concentration on the colder side will increase. Now, the diffusive flow will dominate, and particles will tend to move to the other side. The net particle current density is given by-

$$\mathbf{j} = -D \nabla p(\mathbf{r}) - D_T p(\mathbf{r}) \nabla T \tag{1.13}$$

where $p(\mathbf{r})$ is the probability distribution to find a nanoparticle at a distance $\mathbf{r}$ in the the given temperature gradient. At steady state, $\mathbf{j} = 0$

$$p(\mathbf{r}) = p_0 \exp\left(-S_T \Delta T(\mathbf{r})\right) \text{ where } S_T = \frac{D_T}{D} \tag{1.14}$$

14

S_T is the Soret coefficient of the particle. It is the ratio of the thermal diffusion coefficient with the normal Diffusion coefficient. It can be positive, negative or 0. It scales linearly with the size of the nanoparticle ($S_T \propto R$).

Now $p(\mathbf{r})$ is an exponential function. To understand the effect of temperature in this system, we can compare it to the argument of the exponential in the Boltzmann distribution. This can give us some effective potential energy of the particle in this system.

$$\frac{\Delta E(r)}{k_B T} = S_T \Delta T(r) \tag{1.15}$$

where $E(r)$ is the effective potential energy of the particle. It is to be noted that this system does not have a fixed temperature; therefore, it can never have Boltzmann distribution. From the expression, it is easy to see that if the temperature has extrema, the effective potential energy might also follow the trend.

Thermophoresis can be employed to trap particles at nano-, and mesoscale [16]. Particles with a negative Soret coefficient will get stably trapped at the hotspot. However, most particles have a positive Soret Coefficient, i.e. they drift from a hot region to a cold region. These particles tend to run away from the hotspot, making trapping using a simple architecture impossible. There have been novel approaches to trap such particles using an acousto-optic deflector and advanced computer programming[17]. The position of a particle is monitored in real-time, and the laser spot is deflected such that the particle remains near the desired location. In fact, trapping particles based on thermophoresis has been widely studied. For instance, in figure 1.6 [5], a thermophoretic trap was used to study the fragmentation of a fibril.
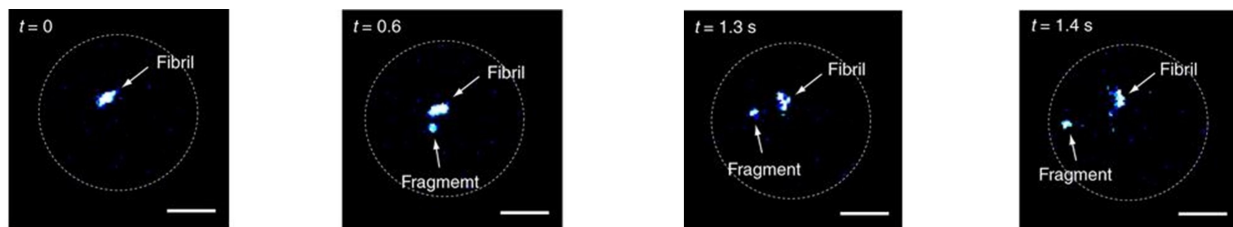
Figure 1.6: Study of a fibril fragmentation in thermophoretic trap. Reproduced from Nature methods vol. 16,7 (2019): 611-614.[5]

The capabilities of a thermophoretic trap are not just limited to single particle trapping.

Our group has shown large-scale assembly of silica beads[6].
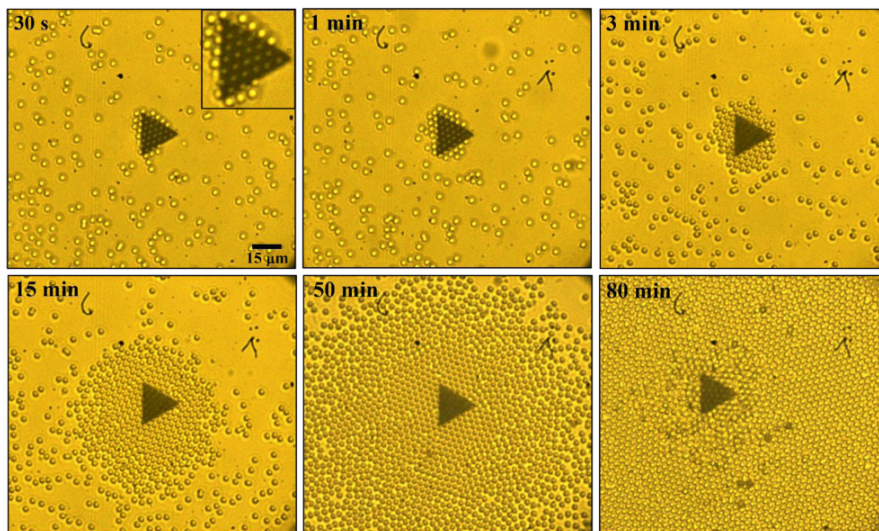
Figure 1.7: Our group has shown a large scale assembly of silica microsphere formed due to optical heating of gold microtriangle. Reproduced from J. Phys.: Condens. Matter 32 324002 [6].

1.5   Surface Enhanced Raman Scattering

The inelastic interaction of photons with matter is termed Raman Scattering. During this process, there is a change in the energy and momentum of photons. Since Raman peaks are unique to every molecule, it is considered to be its molecular signature [18]. Unlike fluorescence, Raman scattering can occur with resonant as well as for non-resonant radiation. When non-resonant radiation hits a molecule, the electron is raised to a "virtual" state, which is extremely short-lived. Now, if the electron comes back to the same state, it will emit a photon of the same wavelength, and this scattering will be elastic in nature (Rayleigh scattering). Raman scattering happens when the electron in the "virtual" state settles in a different vibrational state. If it goes to a higher vibrational state, the line obtained is red shifted and is often called Stokes shift. If it goes to a lower vibrational state, the line obtained is blue-shifted and is called anti-Stokes shift. When resonant radiation is incident on the molecule, there are two competing processes that can occur-Fluorescence and Raman scattering. In general, the cross-section of fluorescence is about 10^{14} times higher than

16

the cross-section of Raman scattering. Therefore, Raman scattering is often not detected. To enhance the Raman signal and overcome this issue, one uses surface-enhanced Raman scattering (SERS).

When molecules come close to the surface, the Raman signals are enhanced, and this enhanced scattering is called surface-enhanced Raman scattering (SERS). Signal, by SERS, can be in general be boosted up to 10^{14} times [19] and is enough to be detected even in the presence of fluorescence. Surface enhancement can occur by two mechanisms — Chemical enhancement and Electromagnetic enhancement. In chemical enhancement, the electronic interaction between the adsorbed molecule and the surface boosts the signal. In electromagnetic enhancement, the enhanced electric fields in the vicinity of metal nanostructures lead to boosting of the Raman signal. Electromagnetic enhancement is proportional E^4, where is E is the electric field. Chemical enhancement is generally orders of magnitude weaker than electromagnetic enhancement.

1.6   Motivation for the work

There has been tremendous effort in the direction of creating assemblies of dielectric particles[6], [20], [21]. Creating large scale assemblies of metal nanoparticles is of great interest. Such assemblies have enhanced local electric fields in the vicinity that can be exploited for various applications[22],[23],[24].

Using conventional optical tweezers for this purpose pose multiple difficulties. Metals are good scatterers, and the gradient force required to dominate scattering force requires enormous power densities. Furthermore, high operating laser power heats the metal, thus destabilizing the trap. Metals, gold nanoparticles in particular do not get trapped by thermophoresis using a simple architecture.

One of the methods to self-assemble metal particles is by employing surfactant-based optothermal trapping. This method was first demonstrated by L. Lin et al. in their 2016 paper[25]. There have been subsequent works by the same group to push the limit of optothermoelectric trapping and demonstrate its capabilities [26], [8], [27]. Other groups have shown the usage of such traps [28] and suggested improvisations [29] to its trapping capability.

This is a relatively recent technique and has multiple questions that still need to be answered. For instance, there is no clear theory about particle-solvent interaction in such a system; predicting values for surfactant concentration for a given particle assembly from first principles is challenging. In this thesis, we elaborately study various factors that play a role in optothermoelectric agglomeration of nanoparticles. We study the effect of changing power density on the sample, the wavelength of excitation, coating on nanoparticle and Raman scattering enhancement capability of such assembly.

In Chapter-1, we discussed the preliminaries necessary to understand the problem. Plasmonics and localized surface plasmon resonance lie at the heart of optical heating. We discussed how a metal particle could act as a nanoscale heat source. We also discussed the most basic form of optical trapping, an ingenious invention, which won the Noble Prize in 2018. The chapter is concluded with a preliminary discussion about thermophoresis, SERS and the motivation for undertaking this project.

In Chapter-2, we first describe the synthesis protocols for various metallic colloids and gold microplates. Details of parameters to produce a thin gold film using thermal vapour deposition is also discussed. We move on to the techniques section, where we describe the dark field microscopy and particle tracking methods used in this thesis.

In Chapter-3, we explain the main results of the thesis. We discuss the system, optical setup and sample preparation necessary to get started with the agglomeration of the particles. Next, we talk about the mechanism of the assembly formation of gold nanoparticles. Observation of agglomeration and disintegration is presented along with the calculation of ensemble mean square displacement. We move on to explain the effect of various parameters in the problem, including surfactant concentration, power density, wavelength, and coating. We end this section by discussing the Raman spectra of rhodamine 6G enhanced by the particle assembly.

In Chapter-4, we conclude the thesis and establish its significance in terms of future work coming out of this project.

Chapter 2

Chemical synthesis, characterization and experimental techniques

In this chapter, we outline the materials and methods used in this dissertation. In the first section, the synthesis of metallic colloids, including citrate reduced gold nanoparticles, citrate reduced silver particles, and core-shell particles, is presented. Characterizations including UV-Visible Spectroscopy and FE-SEM imaging were done, and individual results are discussed. In the next section, we discuss the synthesis of single-crystalline gold microplates. Then we outline the synthesis protocol for thin gold films synthesized using thermal vapour deposition. Finally, two of the main techniques applied are briefly discussed, namely, dark field microscopy and particle tracking.

2.1   Synthesis of metallic colloids

The assembly of gold and silver nanoparticles is the central theme of this thesis. For many of the experiments on trapping and tracking of the metal colloids, commercially available metal colloids were used as absolute control of shape and size over a very large number of particles was required. However, the stabilizing agents coated on the surface of such 'off-the-shelf' colloids often limit their ability to be trapped in an optothermoelectric field and enhance Raman scattering peaks.

It has been shown that metallic colloids prepared by citrate reduced method provide large enhancement in the electric field and are the best choice for surface-enhanced Raman spectroscopic measurements [30],[31],[32]. In this section, we'll outline the protocol to prepare Lee, and Misel citrate reduced metal nanoparticles, which were first synthesized by P.C. Lee and D. Misel in 1982 [33]

2.1.1   Citrate reduced Gold Nanoparticles

Chemicals -Gold Chloride Trihydrate ($HAuCl_4.3H_2O$), Trisodium citrate ($Na_3C_6H_5O_7$), milli-Q water

Synthesis 480 mg of ($HAuCl_4.3H_2O$) was dissolved in 1000 mL of water. The solution was continuously stirred using a magnetic stirrer and it was brought to boiling. 100 mL of 1% Trisodium citrate (by weight)was added, and the boiling was continued for 1 hour. Detailed protocol is mentioned elsewhere [33], [34].

The solution obtained had a wine-red coloration. The FESEM image of the particles shows that the approximate particle size was less than 40 nm. The UV-Vis absorption spectra have a peak at 525 nm.
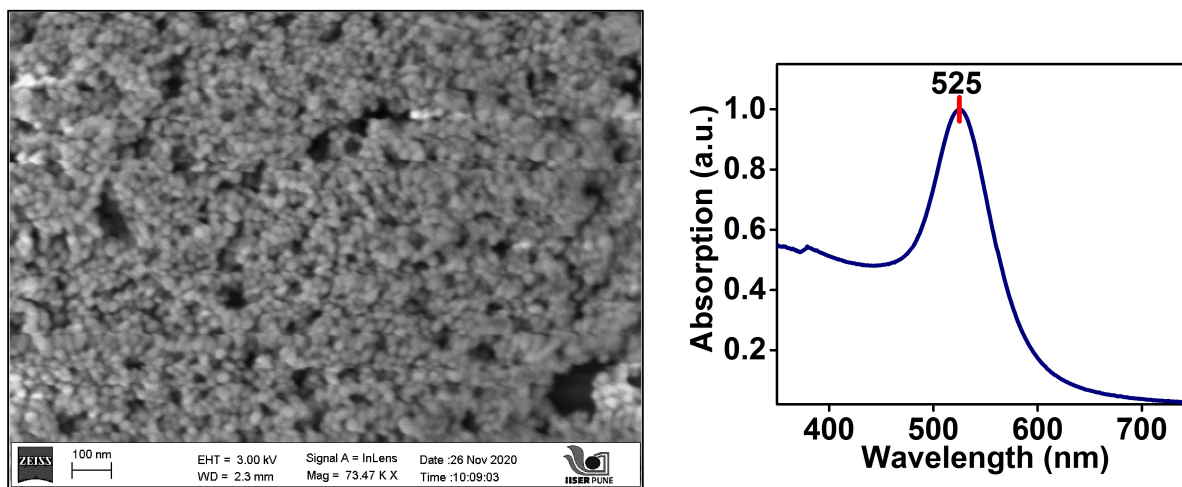
Figure 2.1: Scanning electron microscope (SEM) image and UV-Visible absorption spectrum of citrate reduced gold nanoparticles. The approximate particle size is less than 40 nm. The plasmon peak of the particles is at 525 nm.

2.1.2   Citrate reduced Silver Nanoparticles

Chemicals - Silver Nitrate($AgNO_3$), Trisodium Citrate ($Na_3C_6H_5O_7$), milli-Q water

Synthesis- 180mg of silver nitrate ($AgNO_3$) was dissolved in 1000 mL of milli-Q water (H_2O) to make a 1.04 mM solution of $AgNO_3$. This solution was brought to boiling. A solution of 10 mL of 1% (by weight) trisodium citrate ($Na_3C_6H_5O_7$) was added while boiling. It serves both as a reducing and stabilizing agent. Boiling was continued for 1 hour and then the solution was brought to room temperature. Detailed protocol is mentioned elsewhere [33], [34] [35].

The final solution had a grey colour. The absorption peak for citrate reduced silver nanoparticles is at 433 nm. The FESEM image of the particles shows that particles have different shapes. The approximate size of the particles ranged from 40 nm to 70 nm.
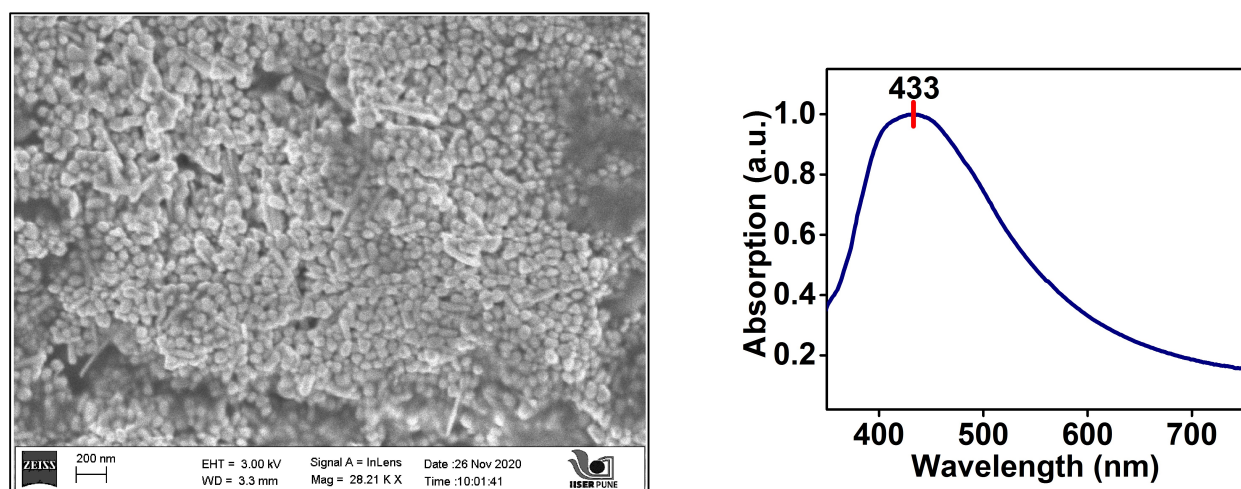
Figure 2.2: Scanning electron microscope (SEM) image and UV-Visible absorption spectrum of citrate reduced silver nanoparticles. The approximate particle size is about 40-70 nm. The plasmon peak of the particles is at 433 nm.

2.1.3   Au$_{shell}$ Particles

Chemicals - Citrate reduced silver nanoparticles prepared by Lee and Misel method, Gold Chloride Trihydrate ($HAuCl_4.3H_2O$),Hydroxylammonium chloride($NH_2OH.HCl$), milli-

21

Q water

Synthesis- To synthesis these particles, we followed the protocol outlined elsewhere [36], [37]. A solution of citrate reduced silver nanoparticles is prepared as per protocol described in the previous section. 12.5 mL of the solution is mixed with 10 mL of water. It is placed on a magnetic stirrer, and stirring is initiated. A solution of 6.25 mM $NH_2OH.HCl$ and 0.465 mM $HAuCl_4.3H_2O$ is prepared. 1.3 mL of $HAuCl_4.3H_2O$ solution is was added dropwise along with an equal volume of $NH_2OH.HCl$ at the rate of 2mL per minute. The stirring was continued for about 45 minutes.

The final solution had a dark grey coloration. The absorption peak in the UV-Vis spectra was at 499 nm. This value is between the gold and silver peaks, which hints that core-shell particles have formed. The shelf life of these particles is very less, as there is no coating of stabilizing agent on their surface. It is advisable to use them within a few days of their preparation.
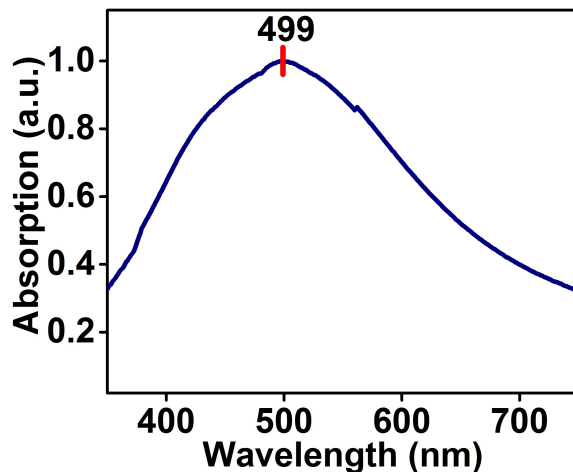
Figure 2.3: UV-Visible absorption spectrum of Au_{shell} particles nanoparticles. The plasmon peak of such shell particles is at 499 nm.

2.2   Preparation of single-crystalline gold microplates

Chemicals - Gold Chloride Trihydrate ($HAuCl_4.3H_2O$), Poly(vinylpyrrolidone) (PVP, MW=40,000)
Synthesis- The synthesis that was followed is mentioned in detail elsewhere [38]. 1mL 0.2
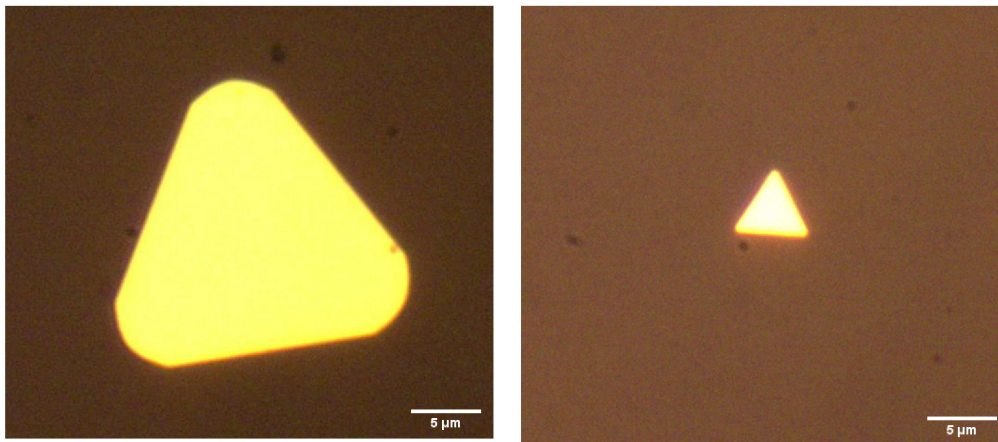
Figure 2.4: Optical images of the single crystalline gold microplates. The plates varied in size from 2-20 μm. Larger plates had more rounded edges, while the smaller ones had sharp edges.

M solution of 1 mL of (HAuCl$_4$) was prepared. This solution was added to 6 mL ethylene glycol. The solution was heated in a beaker and stirred slowly at 150°C. Then 3 mL ethylene glycol solution of poly(vinylpyrrolidone) was injected dropwise. The reaction mixture was continuously heated and stirred. Shining particles began to appear after some time. The solution was kept for heating for about 30 mins. The reaction mixture was diluted with acetone and centrifuged at 4000 rpm for 15 min, and the solvent containing residual reactants was decanted. The products were then rinsed with ethanol and centrifuged repeatedly to remove the possible contamination.

The size of the plates was ranged from 5 μm to 20 μm. The shapes obtained were triangular and hexagonal. Multiple plates had rounded edges. Figure 2.4 shows the optical image of the single-crystalline gold microplates synthesised using this protocol.

2.3 Preparation of Au thin films

Thin metals films are commonly deposited by physical vapour deposition. We used thermal vapour deposition (TVD) to deposit 5 nm thin gold films. First, the coverslips that need to be coated with the metal are placed inside the chamber, and the vacuum pump is turned on. We wait till the pressure in the chamber is $\sim 10^{-7}$ mbar. Once the vacuum is attained, an Inficon SQC310 deposition controller is used to set the following parameters-

Material	Gold
Deposition Rate	0.1 Ås^{-1}
Power	25 %

Table 2.1: Parameters for Thermal Vapor Deposition of 5 nm Au film

After the deposition is complete, the chamber is vented, and the coverslips with desired film thickness are taken out.

To anneal the gold films, they were placed in a furnace at 500° C for 2 hours.
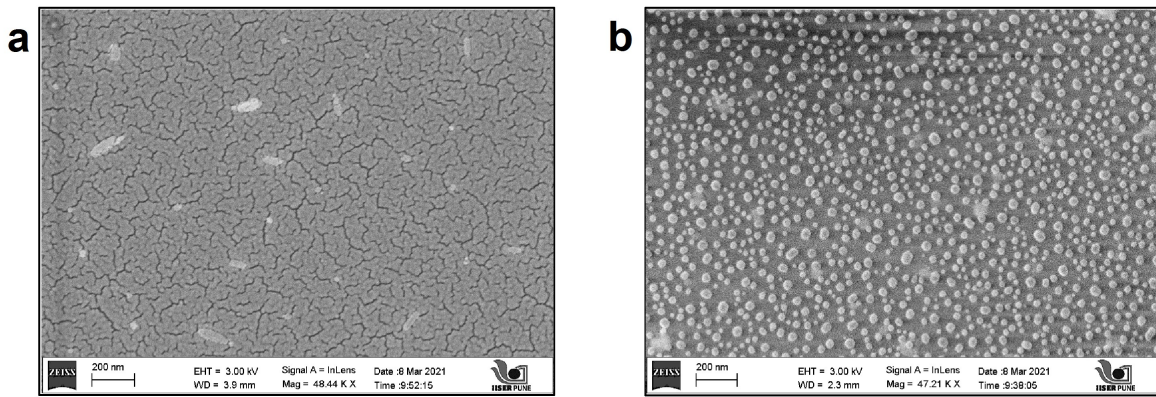
Figure 2.5:   a) Scanning electron microscope (SEM) image of a 5 nm thin gold film produced by TVD b) Scanning electron microscope (SEM) image of an annealed 5 nm thin film (500° C, 2 hours)

2.4 Dark Field Microscopy

Dark field microscopy is an imaging technique where the geometry is such that only the light scattered from the object in focus is collected. All the unscattered light fails to enter the objective lens. Therefore the background in a dark field image appears dark. Such high contrast is very advantageous for further image processing and trajectory analysis. To obtain a dark field image, the following condition must hold true-

$$NA_{condenser} > NA_{objective}$$

The above condition ensures that transmitted light is inclined at a steep angle and does not enter the objective. Metal nanoparticles are strong scatterers in the visible regime. Therefore, they appear brightly coloured on dark background in a dark field image. Their colour is dependent on the plasmon peak of the particle and thus gives information about size, geometry and composition.
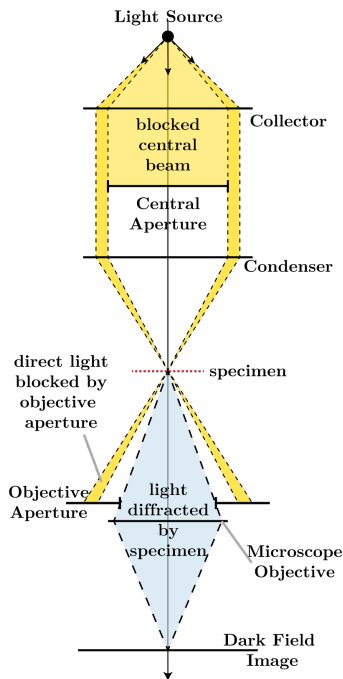
Figure 2.6: Principle of dark field microscopy. The direct light comes at a higher angle and is not collected by the objective. The optical configuration only allows the scattered light to pass. [7]

.

2.5 Particle tracking

Particle tracking is the process of observing the motion of an object over many frames. By particle tracking, one can obtain information about individual particle dynamics (velocity, acceleration etc.) and statistical quantities like diffusion coefficient and mean-squared displacement. It is a process two-step process — Spot detection on high-contrast successive images and linking them to form a particle's trajectory. This thesis is concerned with dark field images of nanoparticles, which are suitable for both single-particle tracking (SPT)and

Multiple Particle Tracking (MPT). The two-dimensional images for particle tracking were recorded using a Thorlabs 224C camera, with a frame rate of 15 frames per second.

For single-particle tracking, we used an ImageJ plugin called MosaicSuite [39]. It was preferred because one can choose the particle of interest, and it gives an annotated video of particle trajectory along with its coordinates. We used this platform to calculate the velocities of individual particles in the trap. This information has been helpful to understand the effect of wavelength on optothermoelectric traps (figure 3.10).

For multiple particle tracking, we employed trackPy[40], a python based routine to track several particles simultaneously. It was preferred for two reasons. First, it tracks a large number of particles across several frames in a short time as compared to Mosaic. Second, it had multiple built-in functions for calculating statistical quantities like mean square displacement of all particles, ensemble mean square displacement etc. We used this platform to calculate the diffusion coefficient of particles when the assembly was disintegrating (figure 3.5)

Chapter 3

Optothermoelectric assembly of metal nanoparticles

Optical manipulation of nanometer-scale objects has multiple applications in nanophotonics and life sciences. As we have seen in section 1.6, assemblies of plasmonic nanoparticles have been shown to many advanced applications. Reversible plasmonic assemblies have been demonstrated via evanescent wave excitation[41]. Other approaches using pH[42],[43], voltage [44] and metal-ion coordination [45] have also been shown.

In section 1.4, we saw how a high NA objective lens could be used to optically trap dielectric beads (For stable trapping $F_{\text{grad}} > F_{\text{scatt}}$). Such optical tweezers provide remote access and real-time information about the trapped bead. However, the optical trapping of metal nanoparticles using gradient force poses some complications.

First, metal nanoparticles in the visible region show enhanced optical absorption and scattering due to their plasmonic resonance. We saw in section 1.3 that intense heat is generated when metal nanoparticles are illuminated near their plasmonic resonance due to the Joule effect. Such heating of particle increases its random motion, thus destabilizing the optical trap. Therefore, stable optical trapping is possible only if we move away from their localized surface plasmon resonance peak. Since most noble metals have their LSPR in the visible regime, one has to use near or mid-IR illumination to trap metal particles.

Second, optical power densities required to achieve a large optical gradient force is roughly

about $10 - 100$ mW/μm^2. Therefore, the biological applicability of such traps is limited because, at such high power, cells and other organelles are irreparably damaged[8]. This power is so high that it might end up damaging the metal particle too.

Finally, when one employs such high power densities, the enhanced scattering cross-section of large metal nanoparticles leads to a very large optical scattering force. Therefore, it is only possible to trap small metal nanoparticles (i.e. dipole approximation holds good).

We saw in section 1.3 how thermophoresis could be utilized to trap dielectric beads. It is possible to form a large scale assembly of colloids using thermoplasmonic heat generation. Recently, L. Lin et al. have extrapolated the idea of temperature- gradient based trapping to metal nanoparticles[25]. They were able to make a large assembly of metal nanoparticles at low power using the heat generated by LSP excitation and differential movement of surfactant ions in a thermal gradient.

This chapter will explore the experiments done to understand the surfactant-based optothermal trapping of gold nanoparticles. We will elaborate on the mechanism of the assembly and understand the parameters in the agglomeration of particles, and determine their threshold values.

3.1 Optical setup

The optical configuration used in our optothermoelectric trapping experiments is shown in Figure-3.1. The laser source used was 633 nm. We put a 5x beam expander lens system before it incidents on the objective lens of a commercial inverted microscope. The objective lenses used in the experiments were 100x, variable NA oil immersion and 100x, 1.49 oil immersion. A detailed description of the preparation of the sample chamber is presented in the following section. White light is also focused on the sample with the condenser. The objective lens collects the scattered light from the sample, and the light passes through a 633 edge filter to block the laser.

Since the NA of the condenser lens is 0.9, we employed two mechanisms to create a dark field image. When the objective lens was used at NA lower than 0.9, one would automatically get a dark field image, as the light incident on higher angles will not be collected. For cases
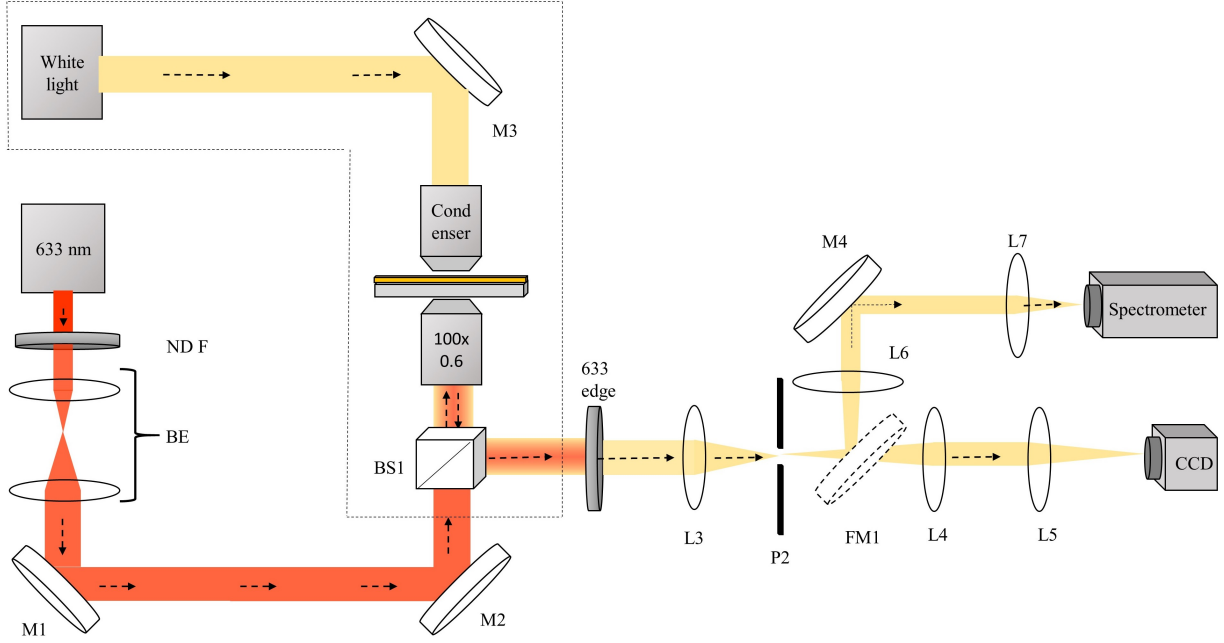
Figure 3.1: Schematic of the optical setup used in the experiment. The backport of the inverted microscope (in the box) is filled by a 633 nm expanded laser beam used to illuminate the Au film in the sample to facilitate optothermoelectric trapping. dark field microscopy is used to visualize the trapped particles. This microscope setup is also coupled to a spectrometer for in-situ SERS.

where we had to use 1.49 NA, we kept a pinhole aperture at the back focal plane of L3. We adjusted the pinhole such that the light coming at higher angles is blocked. The beam that passed through was focused on the camera. We were able to obtain high-quality dark field images using this configuration.

3.2   Sample preparation

To prepare a sample for a typical trapping experiment, first, gold nanoparticles are dispersed in a solution of a CTAC. The size of the nanoparticles and concentration of CTAC depends on the experiment. The solution is put in an ultrasonic bath for about 20 minutes. A spacer is pasted on the thin Au film to form a chamber. The solution is then dropcasted inside the chamber. The chamber is sealed with another coverslip.

Although the trapping experiments can be carried by dropcasting the CTAC-nanoparticle
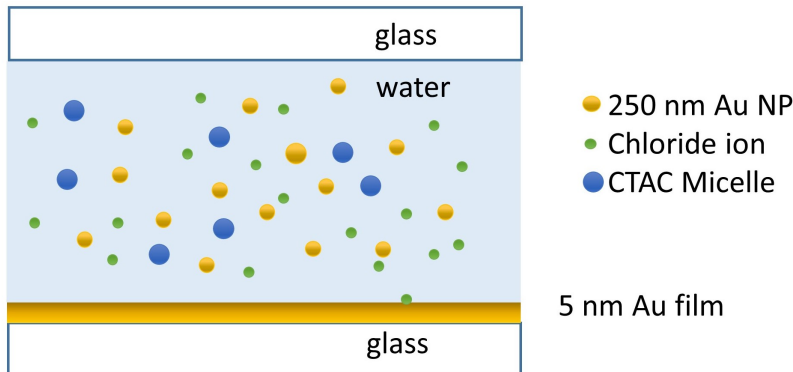
Figure 3.2: Schematic of sample chamber. CTAC micelles and chloride ions are randomly dispersed in the gold colloid solution over a thin gold film.

solution on a glass coverslip/ slide, a sealed chamber offers several advantages. First, the evaporation of the fluid is considerably reduced. Therefore the reading times can be much longer. In our experiments, when we used a glass slide without an upper seal, we noticed that the fluid showed signs of drying within 15 minutes or so. To get longer readings on a sample, it is necessary not to let the fluid evaporate, and thus a chamber is preferred. Furthermore, the chamber allows us to use an oil immersion condenser lens. Finally, the quality of imaging is better with a chamber because there is no curvature of the droplet and light scattering is more uniform.

From our experiments, we also noticed that using chamber configuration to perform spectroscopic measurements posed some challenges. There was a huge fluorescence response when the signal was collected by a 50x, 0.5 NA air objective lens. However, when we used a 60x, 1.2 NA water-immersion lens to collect light from a sample dropcasted on a glass slide, the fluorescence signal was greatly suppressed. We do not understand if it is the increased NA or a difference in sample configuration that resulted in reduced fluorescence. One should be careful and choose the sample configuration according to the aim of the experiment.

3.3 Mechanism of the trap

Optothermoelectric trapping is a low-power technique to create a large scale assembly of nanoparticles. Many physical effects come together to give large to this effect, namely, thermophoresis, thermoplasmonics and thermoelectricity. The subtle interplay of these effects is

briefly described in this section.

First of all, when we disperse the sample in a surfactant solution (here, CTAC) and if the CTAC concentration is above its critical micellar concentration (0.13–0.16 mM), the CTAC molecules self-assemble to form a micelle which is a macro-sized ion. CTAC, being a cationic surfactant, assembles into a positively charged cation. CTAC molecules also get adsorbed on the surface of the gold nanoparticles, imparting a positive charge.

The thin gold film acts as a heat source when illuminated with a laser. For most of the experiments, we have utilised a 633 nm laser. The sample contains positively charged macro-cations of CTAC micelles, positively charged gold nanoparticles with CTAC adsorbed on their surface and the negatively charged chloride ions. Without optical heating, all these ions are randomly distributed in the sample.

In section 1.4, we saw that in the presence of a temperature gradient in a fluid medium, particles show a steady drift on top of their Brownian motion. The steady-state probability distribution of the ions is governed by their Soret Coefficient (S_T). In this case, the Soret coefficient of the species is very different. S_T of Chloride ions $\approx 7 \times 10^{-4} \mathrm{K}^{-1}$ while S_T of Micelles is $\approx 10^{-2}$. This large disparity in Soret Coefficients will lead to a difference in their steady-state distribution in the presence of thermal gradient. When the thin gold film is illuminated by the laser, LSPs are excited, and the film begins to heat locally due to thermoplasmonic effects, as discussed in section 1.2. This optical heating leads to the generation of a thermal gradient in the system. Both the ions experience thermophoresis and move from hot to cold owing to their positive S_T. However, the steady-state distribution of the two ions will be very different. Chlorine ions will be localised near the hotspot, while the CTAC micelles will be more delocalised and move slightly far away from the hotspot. This stationary spatial redistribution of ions gives rise to a steady-state electric field given by-

$$E_T = \frac{k_{\mathrm{B}} T \nabla T}{e} \frac{\sum_i Z_i n_i S_{Ti}}{\sum_i Z_i^2 n_i} \tag{3.1}$$

Here, i indicates the charged ion CTAC micelle and chloride ion, k_B is the Boltzmann constant, T is the temperature of surrounding, ∇T is the temperature gradient, e is the electronic charge, S_{Ti} are the Soret Coefficients of the species, n_i is the concentration, and Z_i is the total charge of the ions.
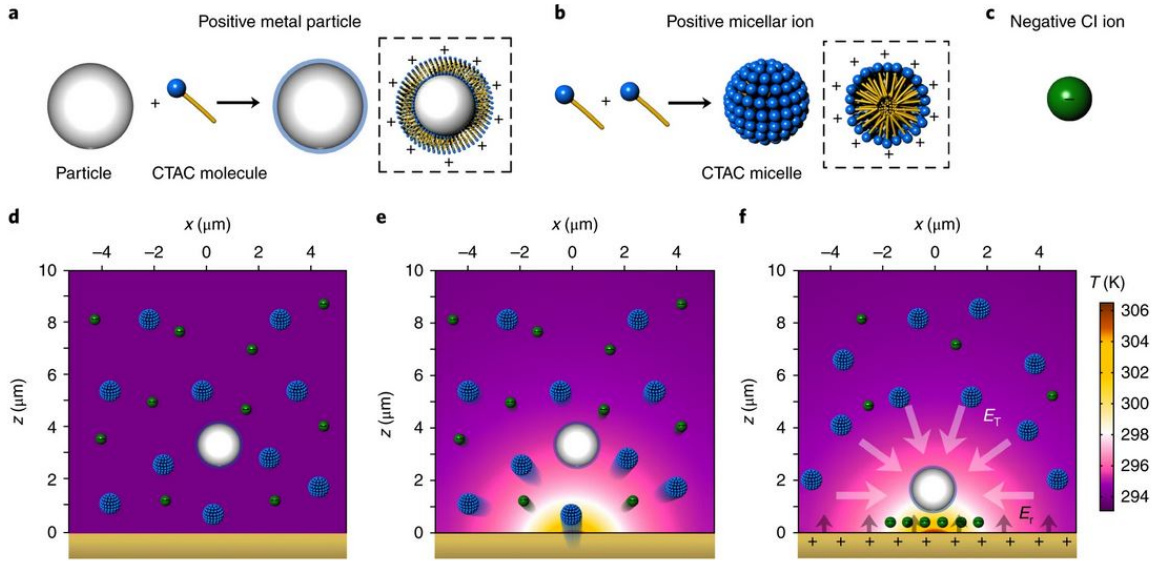
Figure 3.3: Mechanism of optothermoelectric trapping. a) CTAC molecule is adsorbed on the surface of gold nanoparticle and modifies its surface charge b) CTAC molecules self assemble to form micelles c) Negatively charged chloride ion in the solution d) In the absence of thermal gradient all ions are randomly dispersed in the solution e) Gold film is illuminated f) Steady-state distribution of ions lead to the generation of a thermoelectric field which traps the nanoparticle. Reproduced from Nature Photon 12, 195–201 (2018) [8]

.

Since the Soret coefficient is positive, the electric field lines will originate from them and point toward the hotspot, where chlorine is localised. This electric field directs the CTAC adsorbed gold particle towards the hotspot. It is to be noted that the gold film also adsorbs the CTAC molecule. This layer then counters the generated electric field, thus stably trapping the nanoparticle.

3.4 Assembly and disassembly of metal nanoparticles

Experimental Details

A sample chamber was prepared following the protocol mention in section 3.2 with the specifications mentioned in table 3.1.

Particle	250 nm Au
CTAC	10 mM
Wavelength	633 nm
Objective	100x, 0.6 oil-immersion
Power Density	0.18 mW/μm^2

Table 3.1: Experimental specifications to assemble particles

Results
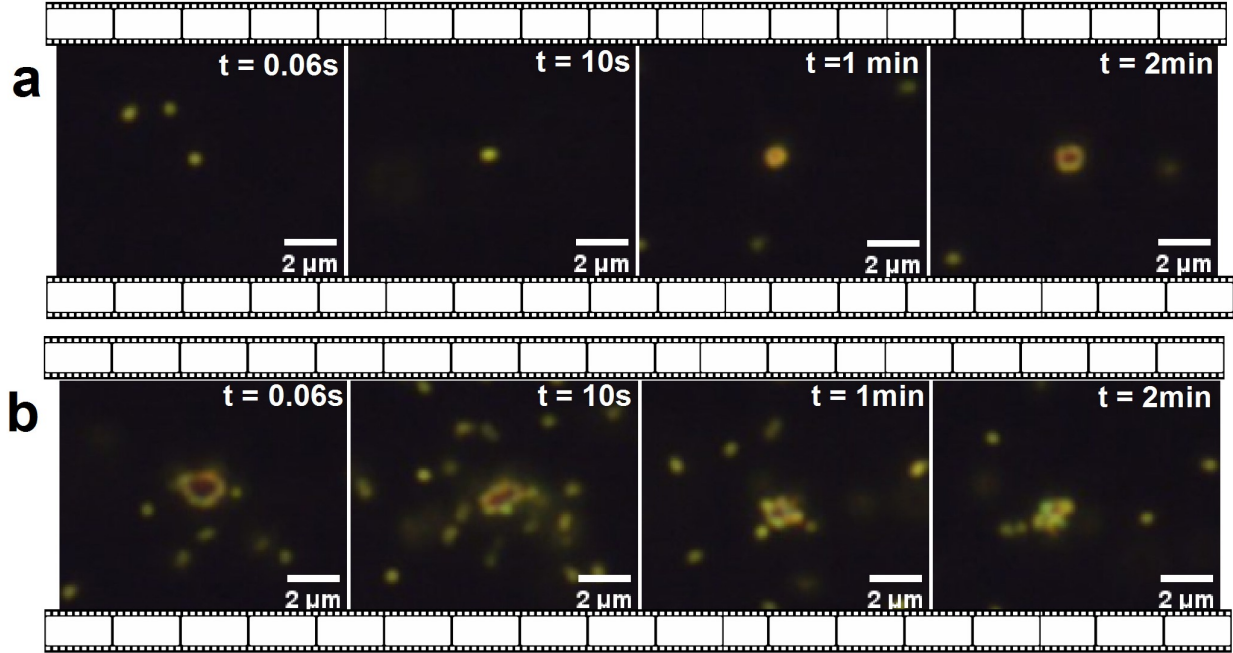
Figure 3.4: a) Successive images show agglomeration of 250 nm Au nanoparticles. Assembly was allowed to form for 15 minutes, and b) Successive images show the disintegration of previously formed assembly.

Figure 3.4a shows the successive images of agglomeration of 250 nm Au nanoparticles. They are trapped at extremely low power, at least 2-3 orders of magnitude lesser than power densities in typical optical trapping experiments. This assembly is also reconfigurable at short time scales. If the particles have been agglomerating for less than a minute, they will immediately start disassembling as soon as the laser is turned off. This has also been reported in [25]. However, if the particles have been agglomerating for $\sim$ 10 minutes, they do not disassemble very quickly. Although the agglomerate will shrink considerably, it will

take a very long time to disassemble completely. The assembly was allowed to form for 15 minutes. Figure 3.4b shows the successive images of the disintegration of the cluster.

3.5   Ensemble Mean Squared Displacement

Particles come together to form an agglomerate as a directed thermoelectric force acts on them. It points towards the hotspot. The trajectory of one such particle is shown in figure 3.10a. However, when particles have formed an agglomerate and if the laser is turned off, there is no external force in the system. The particles will diffuse out of the agglomerate, and we expect them to show Brownian dynamics. The mean square displacement (MSD) of a particle is the deviation of a particle from a reference point over a given time. For a random walker, it gives the measure of the area explored by the particle. For a Brownian particle suspended in a Newtonian fluid, the slope of log MSD vs log lag-time is unity. It is one of the primary characteristics of Brownian motion.

$$\text{MSD} \propto \tau$$

When MSD is averaged over several trajectories, it is called ensemble mean square displacement (EMSD). This section will look at the ensemble mean displacement of the particles when the assembly is disintegrating.

Basic parameter details

The video was acquired for the 250 nm Au nanoparticle disassembly process at a frame rate of 15 frames per second. The particle tracking was done with the trackpy routine in the Jupyter notebook. The minimum mass was 500, and the mask size was 11 px. For the final calculations, only those trajectories were considered, which were at least 100 frames long.

Results and Discussion

It has been shown that as soon as the laser is turned off, the thermal gradient in the system vanishes [3]. In the absence of a thermal gradient, there will not be an electric field to hold the particles together, and hence the assembly starts to break. To verify if the particles going out are exhibiting Brownian dynamics, we tracked the particles, and the results are shown in figure 3.5. Figure 3.5a shows the particles being tracked. Tracking parameters were carefully chosen to avoid spurious detection, off-focus particle detection and assembly detection. We plotted their ensemble mean square displacement with time in figure 3.5b. The slope is nearly 1, which hints that the dynamics are Brownian. We plotted the slope between two consecutive points in the mean square displacement with lag time to understand the deviation in the fitted slope. The results are in figure 3.5c. It can be seen that for a considerable time, the two-point slope is nearly 1. Only at higher values of lag times is a slight error introduced in the calculation due to insufficient data points. The 250 nm Au particles constantly get out of the plane, which makes their tracking difficult. Therefore, data for larger lag times is difficult to obtain. Furthermore, the calculation can be improved by taking data at a faster frame rate and using a higher resolution camera.
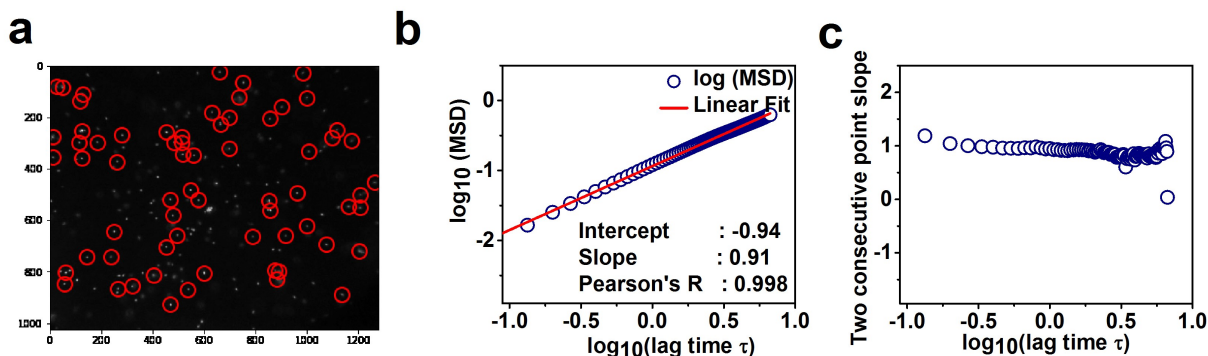

Figure 3.5: a) Annotated frame, red circles denote the particles being detected b) Plot of log-MSD vs log-τ c) two-consecutive point slope

3.6 Effect of surfactant concentration

Surfactant plays a critical role in the assembly of metal nanoparticles. It modifies the surface charge of nanoparticles, thus altering their zeta (ζ) -potential. Since the ζ potential is

a material-dependent property, surfactant concentration must be modified slightly for every nanoparticle to obtain stable trapping. For our experiments we have used cetyltrimethylammonium chloride (CTAC, $C_1 9H_4 2ClN$). As the solvent-particle interfacial effects are not well characterised in literature, it is difficult to predict ζ potential with varying CTAC concentration from theory. Also, many particles of the same material purchased from different vendors have different coatings over them, which makes their ζ potential difficult to predict. The effect of the coating is covered in detail in the next section. In this section, we will understand the role of CTAC and see what is the effect on the agglomeration when its concentration is varied.

Experimental Details

Three sample chambers were prepared as mentioned in the protocol in section 3.2 with varying CTAC concentrations and the specifications mentioned in table 3.2.

Particle	250 nm Au
CTAC	No CTAC, 4mM, 10 mM
Wavelength	633 nm
Objective	100x, 0.6 oil-immersion
Power Density	0.18 mW/μm^2

Table 3.2: Experimental specifications to study the effect of surfactant

Results and Discussion

In the absence of surfactant (here, CTAC), the phenomenon of optothermoelectricity does not take place. As shown in figure 3.6a, no trapping is observed in such a case. Further, at a very low concentration of the surfactant, the thermoelectric field developed is not sufficient to overcome the Brownian motion of the nanoparticles and trap them. However, even in such cases, particles near the laser spot show increased interactions with one another. This is shown in figure 3.6b, where the particles exist as temporary dimers. It is to be noted that such dimers are transient and fade off at the next instant, and new ones are formed. The dynamics of the particles is visibly affected, but the electric field is not strong enough to arrest them at the hotspot. This interaction increases progressively with increased CTAC concentration. Beyond a particular concentration, particles begin to be stably trapped, as

36
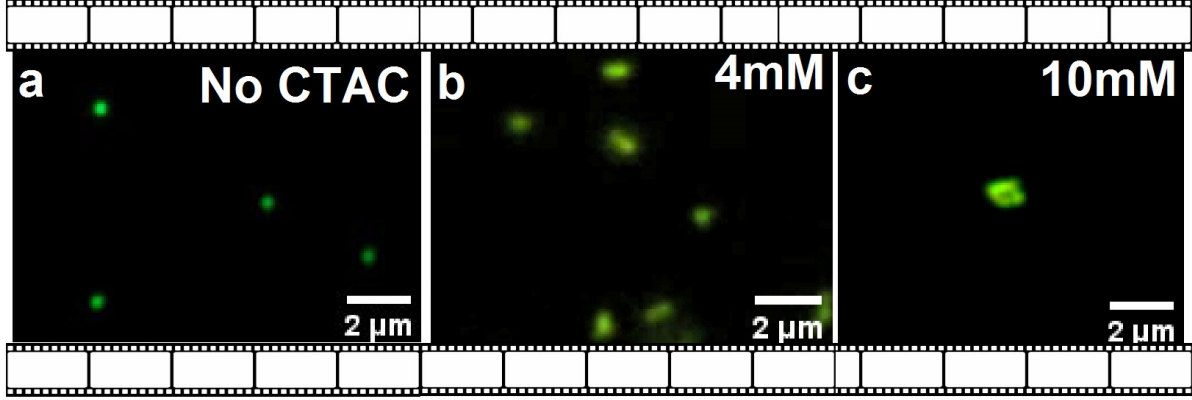
Figure 3.6: Images of optothermoelectric trap after 4 minutes of laser illumination for different samples with varying CTAC concentrations. a) No CTAC, no effect on particle dynamics observed b) 4 mM, particles start showing transient dimers which dissociate fast c) 10 mM, particles get trapped

shown in figure 3.6c. We were able to trap Au nanospheres dispersed in a 10 mM solution. There exists a range of CTAC concentration in which the particle can be trapped stably. For 250 nm Au particle, we observed that the range was from 10 mM to 16 mM. When the CTAC concentration is increased beyond this value, the motion of the majority of the diffusing particles is arrested, and they appear to be stuck on the substrate.

3.7   Effect of power density

Operating power is one of the key determining factors in the choice of tweezers one can employ. If one has to trap metal particles using conventional optical tweezers is about 10-100 $\mu W/\mu m^2$. The typical power density required to trap metal nanoparticles via surfactant-based optothermal tweezers is at least two orders of magnitude less than conventional gradient force-based optical trapping. This low optical power operation is one of the major advantages of such optothermal traps.

   Power density on the sample is given as-

$$\text{Power Density}(P_D) = \frac{\text{Total Power Incident on the sample}}{\text{Area of the focused beam spot}}$$

Also, the diameter of the focused beam spot is determined by the Numerical Aperture (N.A.)

of the objective lens.

$$\text{Diameter of the focus spot} = \frac{0.61\lambda}{\text{N.A.}}$$

Therefore, there are two ways in which power density on the sample can be varied.

- By changing the total power on the sample. This does not modify the size of the focus spot.

- By changing the numerical aperture of the objective lens. The higher the numerical aperture, the higher is the power density on the sample

In this section, we will understand how power density affects the agglomeration of particles. We will see how changing the absolute power incident on the sample has a different effect than just reducing the focused beam spot by increasing NA.

Experimental Details

We performed two series of experiments to understand the effect of power density. In the first series of experiments, we introduced neutral density filters in the 633 nm laser beam path to reduce the total power incident on the sample. Sample chambers were prepared according to the protocol mentioned in section 3.2. Experimental specifications are mentioned in table 3.3

Particle	250 nm Au
CTAC	10 mM
Wavelength	633 nm
Objective	100x, 0.6 oil-immersion
Total Power	0.001mW,0.08mW,0.16mW

Table 3.3: Experimental specifications to study the effect of total power on the sample

In the second series of experiments, the total power incident on the sample was kept the same, 0.16 mW. However, we performed the experiment with different 100x oil-immersion objective lenses with NA=0.6, 0.9 and 1.49, respectively. Sample chambers were prepared according to the protocol mentioned in section 3.2. Experimental specifications are mentioned in table 3.4

Particle	250 nm Au
CTAC	10 mM
Wavelength	633 nm
Objective	100x, Variable NA (0.6-0.9), 100x 1.49 oil-immersion
Total Power	0.16mW

Table 3.4: Experimental specifications to study the effect of changing numerical aperture

Results and Discussion

Figure 3.7 shows the results of the first series of experiments. Here power density was varied by changing the total incoming power onto the substrate. First of all, without laser illumination, the thermal gradient is not generated. As a result, there is no differential movement of the ions in the solution, and thus no electric field is produced. Therefore, no trapping is observed. Likewise, shining very low laser power on the metal film also does not result in trapping, as the temperature gradient is not enough to create a strong thermoelectric field (E_T) to facilitate the trapping of nanoparticles. In our experiments, we observed that for all power density below 0.09 mW/μm^2, trapping was not observed. However, when the power density was increased to 0.18 mW/μm^2, the particles were agglomerated. Therefore, the threshold power density required to initiate must lie between 0.0 9mW/μm^2 and 0.18 mW/μm^2. This bound could not be further tightened due to the unavailability of appropriate neutral density filters at the time of the experiment.
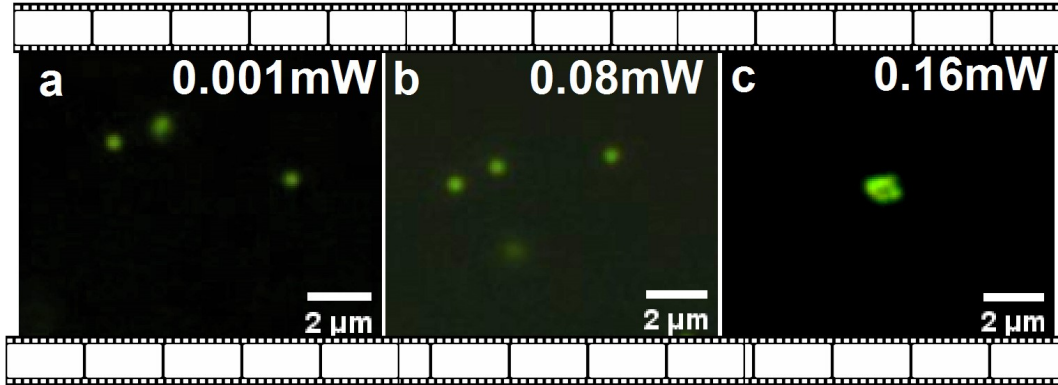

Figure 3.7: Varying the total optical power of 633 nm laser on the sample. a) No assembly at 0.001 mW b) No assembly at 0.08 mW c) Agglomeration of particles at 0.16 mW. All images are taken after about 2 minutes of laser illumination.

Figure 3.8 shows the results of the second series of experiments, where the total power incident on the sample was kept the same (0.16 mW). However, we performed the experiment with different 100x oil-immersion objective lenses with numerical aperture 0.6, 0.9 and 1.49, respectively. We observe that the particles were trapped at all the numerical apertures, and the total size of the assembly is independent of the objective lens. Using a higher NA objective lens, the image's resolution improves drastically, as evident from the image in figure 3.8. However, as the NA increases, the scattering force due to the laser beam experienced by the nanoparticle increases drastically. Therefore, we believe that trapping nanoparticles with a higher numerical aperture objective lens will be difficult with a lower CTAC concentration, as the scattering forces will dominate the thermoelectric field.
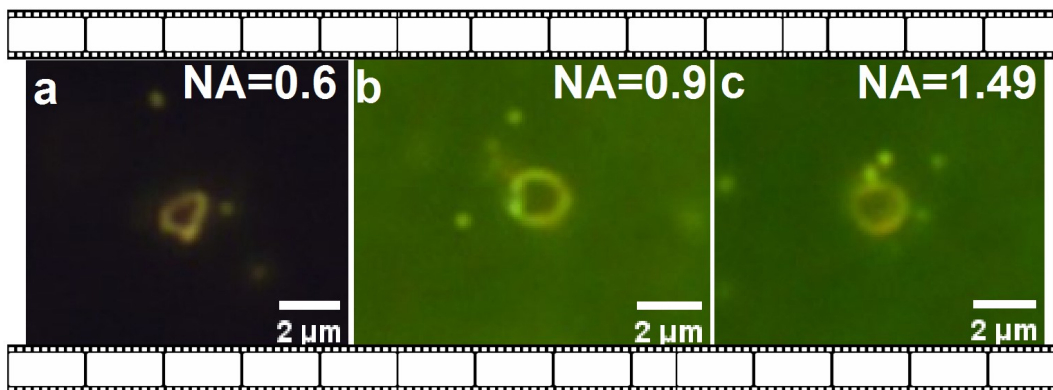
Figure 3.8: Varying the numerical aperture (NA) of the objective lens. a) Agglomeration of particles when NA is 0.6 b) Agglomeration of particles when NA is 0.9 c) Agglomeration of particles when NA is 1.49. All images are taken after about 15 minutes of laser illumination.

3.8   Effect of laser wavelength

In section 1.1, we saw that the light that is incident on a gold nanoparticle oscillates the free electrons. If the excitation wavelength is near the plasmon peak, the resonance condition is fulfilled, and due to Joule heating, the particle heats up very efficiently. The same is true for gold film, which is the heat source in optothermoelectric traps. Figure 3.9 shows the scanning electron microscopy image of the gold film. The cracks on the surface are apparent. A perfectly smooth gold film, being a good heat conductor, would not have facilitated a temperature gradient, thus making optothermoelectric trapping difficult.
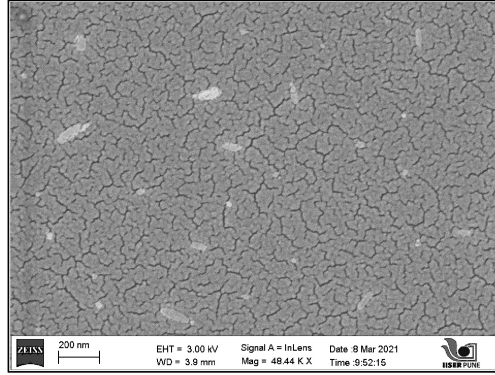
Figure 3.9: Large number of cracks on the surface of 5 nm Au film prepared with Thermal Vapour Deposition are the reason for heat localisation, and thus generation of thermal gradient due to plasmonic heating.

Like every plasmonic structure, this gold film also has an absorption maximum at 526 nm. In this section, we'll understand how the trap gets influenced when the film is illuminated by different wavelengths which are near or far from the plasmon resonance peak.

Experimental Details

Sample chamber was prepared according to the protocol in section 3.2 with the following specifications.

Particle	250 nm Au
CTAC	10 mM
Wavelength	532 nm, 633 nm
Objective	100x, 0.6 oil-immersion

Table 3.5: Experimental specifications to study the effect of wavelength

Individual particles were tracked using the MosaicTrack plugin of ImageJ software. Trajectories were analysed using MATLAB.

41
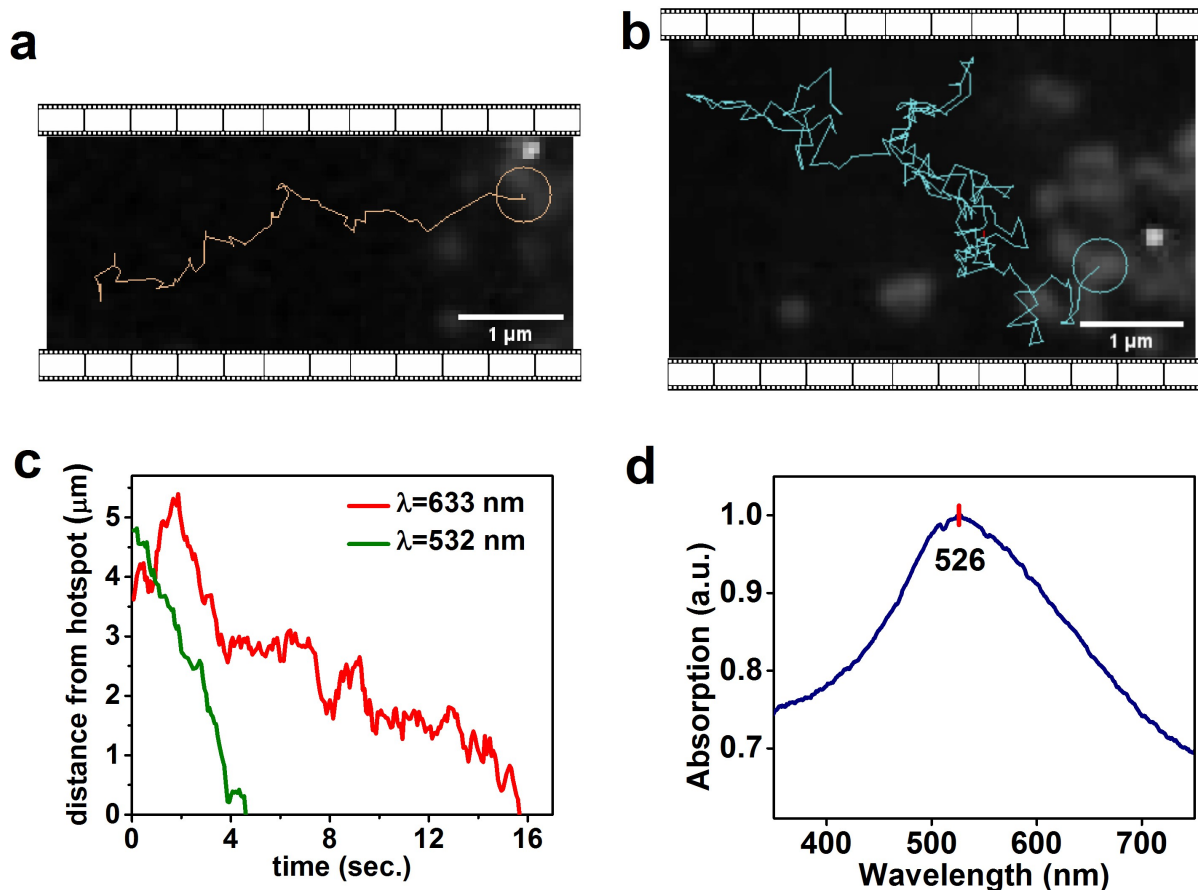
Figure 3.10: a) A particle is moving into the trap when illuminated by a 532 nm laser. b) Particle moving into the trap when illuminated by 633 nm laser. c) Plot of distance from hotspot as a function of time. It clearly shows that particle gets trapped faster with 532 nm laser as compared with 633 nm laser. d) UV-Visible absorption spectra of the gold film. The plasmon peak of the film is at 526 nm.

Results and Discussion

In this optothermal trapping experiment, the illuminated gold film serves as the heat source. To study the effect of wavelength, we tracked the trajectories of the particles in the trap. Figure 3.10a and 3.10b show images of particles that started roughly about 4 μm away from the trap. From figure 3.10c, it can be easily seen that the particle illuminated by 532 nm reaches the trap much faster than the one illuminated by 633 nm, which explores much more area before getting trapped. Therefore, the trap created by 633 is weaker in comparison to the one created by 532 nm.

Localized and surface plasmon are excited by the laser, and the oscillation of the electrons leads to Joule heating, thus increasing temperature. The closer we are to the resonant peak of the plasmons, the faster electrons will oscillate, thus leading to greater heating. The UV-vis absorption spectra of the film are shown in figure 3.10d. It peaks at 526nm, which is near the 532nm laser. Also, it is to be noted that the power density of 532 nm was higher than the power density of 633 nm. Together with both the reasons, we expect a 532 nm laser to be a better heat source for the films we used. This explains our experimental observation.

3.9 Effect of coating on the nanoparticle

Micelle formation on the metal nanoparticle plays a very crucial role in its trapping. It modifies the surface charge and enables it to experience the trapping electric field. However, commercially purchased nanoparticles are often coated with a polymer. The vendors sometimes do not disclose such coating. Although most of these particles can still be trapped, some particles are not at all agglomerated. We believe that this is due to the coating present on the particle, which hampers the micelle formation over the particle. Silver Particles [8] have been shown to be easily trapped. However, the PVP functionalized 200 nm Ag nanospheres (purchased from Sigma Aldrich) were not trapped at all. Some of the coatings which do not hamper the trapping process are citrate coated, PVP, and PBS coated particles.

3.10 Surface enhanced Raman Scattering (SERS) with the assembly of particles

As we saw in section 1.5, SERS is a technique to boost the Raman signal, which is otherwise very weak. For surface enhancement, there are two mechanism — Electromagnetic enhancement and Chemical enhancement. Here we'll focus only on electromagnetic enhancement. It occurs due to enhanced electric field in the vicinity of metal nanostructures.

In this section, we will explore the possibility of enhancement of the Raman scattering signal due to the agglomeration of the particles.

Experimental Details

Sample chamber was prepared according to the protocol in section 3.2 with the specifications mentioned in the following table.

Particle	100 nm Au
CTAC	12 mM
Wavelength	633 nm
Objective	50x, 0.5 air
Dye Molecule	Rhodamine 6G 0.01 mM

Table 3.6: Experimental specifications to take SERS of 0.01mM Rhodamine 6G

Results and Discussion
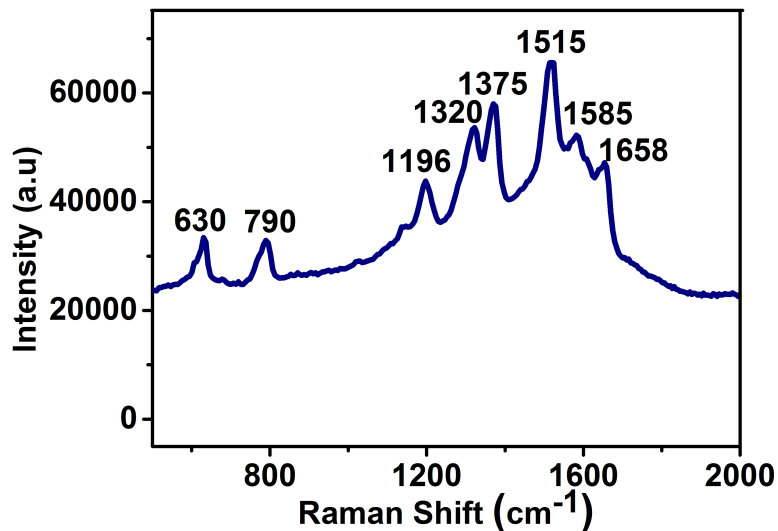
Figure 3.11: Raman scattering spectrum of Rhodamine 6G

The assembly of plasmonic particles provides a large area for multiple SERS hotspots where the electric field is highly enhanced. Figure 3.11 shows the scattering spectrum of rhodamine 6G, which was the target molecule. Spectra were acquired for 2 sec. 633 nm laser was employed to assemble the particles as well as take the scattering spectra. We were able

to obtain the major peaks of the rhodamine 6G molecule. Thus the assembly was able to enhance the Raman signal sufficiently.

It is to be noted that CTAC forms a layer over the metal nanoparticles and aids in large scale agglomeration. However, this layer hampers the electric field enhancement capability of the nanoparticles. These two competing factors should be considered when choosing a CTAC concentration for using this plasmonic substrate for SERS.

Chapter 4

Conclusion and Future Work

Reversible assemblies of plasmonic nanoparticles have locally enhanced electric fields and have multiple applications. Such assemblies have been shown to form by various approaches including evanescent excitation [41], pH [42], [43], voltage [44] and metal-ion coordination [45]. In this project, we explored one-way such assembly can be made – the optothermoelectric trapping of metal nanoparticles. We understood the trap mechanism and explored the role of various parameters in forming a plasmonic assembly. We found out that there is an optimum surfactant concentration in which the trap is functional. At a lower concentration, there is no agglomeration, and at a higher concentration, the motion of the particles is arrested. A similar threshold was found for total power incident in the sample. We also found that the 532 nm wavelength was able to trap particle more efficiently and faster than the 633 nm wavelength laser. We explained this observation using the UV-Vis absorption spectra of the gold film and the total power density incident on the sample. We explored the possibility of measuring Raman spectra of 0.01 mM rhodamine 6G via the plasmonic agglomerate.

This project laid the foundation for future projects that are being carried out in our lab. One direction that is being pursued is to replace the heat source in the sample chamber with something that can be easily prepared. It takes about 24-36 hours to get a few films using thermal vapor deposition. This considerably reduces the pace of experiments being done and also makes the architecture more complex. Furthermore, for thin films, even if there is an error of a couple of nanometers while TVD preparation, it can cause huge errors

in experiments. Finally, a major limitation with using the film is the inability to study the emission from trapped particles because of the background emission from a metallic substrate. After having understood the basic principles of optothermoelectric trapping, we are exploring other heat structures that can be utilised to trap metal nanoparticles. We have successfully been able to form such assemblies using a single metal nanoparticle by exciting it at its plasmon peak. We have been getting promising results in this direction.

Another direction which we are exploring is the possibility of single-molecule detection using such reversible plasmonic assembly. In section 3.10, we have already seen that such metal nanoparticle aggregate has the potential to enhance the Raman scattering signal. We are trying to push the limit of detection and obtain single-molecule surface-enhanced Raman scattering (SM-SERS). Direct illumination of the metal nanoparticle is used to achieve both the plasmonic assembly and SM-SERS sensitivity. There are encouraging results in this direction, and we are taking it forward.

During the course of this thesis, we came across multiple unanswered questions which still need to be explored. For instance, when the laser is kept on for a long period of time, the aggregate doesn't dissociate quickly. It does disintegrate and reduces to a small fraction of its original size; however, it doesn't dissociate quickly in the observation time. The systematic study must be undertaken to understand particle-particle interaction in such assembly. Second, how to theoretically get an optimum CTAC concentration at which particles will get trapped. A clear theoretical description of particle-solvent interfacial effects in optothermoelectric assembly is unavailable. Optothermoelectric trapping of metal nanoparticles is a relatively recent technique and has quite a lot of rich physics which still needs to be studied.

Bibliography

[1] G. Baffou, *Nanoplasmonics*, p. 1–35. Cambridge University Press, 2017.

[2] Wikipedia contributors, "Localized surface plasmon — Wikipedia, the free encyclopedia." `https://en.wikipedia.org/w/index.php?title=Localized_surface_plasmon&oldid=1002479206`, 2021. [Online; accessed 2-May-2021].

[3] G. Baffou, *Thermodynamics of Metal Nanoparticles*, p. 36–80. Cambridge University Press, 2017.

[4] `https://www.laser2000.co.uk/applications/optical-tweezers`, 2021. [Online; accessed 12-May-2021].

[5] M. Fränzl, T. Thalheim, J. Adler, D. Huster, J. Posseckardt, M. Mertig, and F. Cichos, "Thermophoretic trap for single amyloid fibril and protein aggregation studies," *Nature methods*, vol. 16, no. 7, pp. 611–614, 2019.

[6] V. Sharma, D. Paul, S. K. Chaubey, S. Tiwari, and G. P. Kumar, "Large-scale optothermal assembly of colloids mediated by a gold microplate," *Journal of Physics: Condensed Matter*, vol. 32, no. 32, p. 324002, 2020.

[7] Wikipedia contributors, "Dark-field microscopy — Wikipedia, the free encyclopedia." `https://en.wikipedia.org/w/index.php?title=Dark-field_microscopy&oldid=1016072717`, 2021. [Online; accessed 13-May-2021].

[8] L. Lin, M. Wang, X. Peng, E. N. Lissek, Z. Mao, L. Scarabelli, E. Adkins, S. Coskun, H. E. Unalan, B. A. Korgel, *et al.*, "Opto-thermoelectric nanotweezers," *Nature photonics*, vol. 12, no. 4, pp. 195–201, 2018.

[9] A. Ashkin, J. M. Dziedzic, J. E. Bjorkholm, and S. Chu, "Observation of a single-beam gradient force optical trap for dielectric particles," *Optics letters*, vol. 11, no. 5, pp. 288–290, 1986.

[10] A. O. Govorov and H. H. Richardson, "Generating heat with metal nanoparticles," *Nano today*, vol. 2, no. 1, pp. 30–38, 2007.

[11] A. Ashkin, "Acceleration and trapping of particles by radiation pressure," *Physical review letters*, vol. 24, no. 4, p. 156, 1970.

[12] M. J. Lang, P. M. Fordyce, A. M. Engh, K. C. Neuman, and S. M. Block, "Simultaneous, coincident optical trapping and single-molecule fluorescence," *Nature methods*, vol. 1, no. 2, pp. 133–139, 2004.

[13] A. Ishijima, H. Kojima, T. Funatsu, M. Tokunaga, H. Higuchi, H. Tanaka, and T. Yanagida, "Simultaneous observation of individual atpase and mechanical events by a single myosin molecule during interaction with actin," *Cell*, vol. 92, no. 2, pp. 161–171, 1998.

[14] C. G. Galbraith and M. P. Sheetz, "Keratocytes pull with similar forces on their dorsal and ventral surfaces," *The Journal of cell biology*, vol. 147, no. 6, pp. 1313–1324, 1999.

[15] D. G. Grier, "Optical tweezers in colloid and interface science," *Current opinion in colloid & interface science*, vol. 2, no. 3, pp. 264–270, 1997.

[16] M. Braun and F. Cichos, "Optically controlled thermophoretic trapping of single nano-objects," *ACS nano*, vol. 7, no. 12, pp. 11200–11208, 2013.

[17] M. Braun, A. Würger, and F. Cichos, "Trapping of single nano-objects in dynamic temperature fields," *Physical Chemistry Chemical Physics*, vol. 16, no. 29, pp. 15207–15213, 2014.

[18] K. Kneipp, H. Kneipp, and H. G. Bohr, "Single-molecule sers spectroscopy," *Surface-Enhanced Raman Scattering*, pp. 261–277, 2006.

[19] K. Kneipp, Y. Wang, H. Kneipp, L. T. Perelman, I. Itzkan, R. R. Dasari, and M. S. Feld, "Single molecule detection using surface-enhanced raman scattering (sers)," *Physical review letters*, vol. 78, no. 9, p. 1667, 1997.

[20] S. Furumi, H. Fudouzi, and T. Sawada, "Self-organized colloidal crystals for photonics and laser applications," *Laser & Photonics Reviews*, vol. 4, no. 2, pp. 205–220, 2010.

[21] M.-P. Valignat, O. Theodoly, J. C. Crocker, W. B. Russel, and P. M. Chaikin, "Reversible self-assembly and directed assembly of dna-linked micrometer-sized colloids," *Proceedings of the National Academy of Sciences*, vol. 102, no. 12, pp. 4225–4229, 2005.

[22] N. J. Halas, S. Lal, W.-S. Chang, S. Link, and P. Nordlander, "Plasmons in strongly coupled metallic nanostructures," *Chemical reviews*, vol. 111, no. 6, pp. 3913–3961, 2011.

[23] T. B. Hoang, G. M. Akselrod, C. Argyropoulos, J. Huang, D. R. Smith, and M. H. Mikkelsen, "Ultrafast spontaneous emission source using plasmonic nanoantennas," *Nature communications*, vol. 6, no. 1, pp. 1–7, 2015.

[24] Z. Zhu, W. Liu, Z. Li, B. Han, Y. Zhou, Y. Gao, and Z. Tang, "Manipulation of collective optical activity in one-dimensional plasmonic assembly," *ACS nano*, vol. 6, no. 3, pp. 2326–2332, 2012.

[25] L. Lin, X. Peng, M. Wang, L. Scarabelli, Z. Mao, L. M. Liz-Marzan, M. F. Becker, and Y. Zheng, "Light-directed reversible assembly of plasmonic nanoparticles using plasmon-enhanced thermophoresis," *ACS nano*, vol. 10, no. 10, pp. 9659–9668, 2016.

[26] L. Lin, J. Zhang, X. Peng, Z. Wu, A. C. Coughlan, Z. Mao, M. A. Bevan, and Y. Zheng, "Opto-thermophoretic assembly of colloidal matter," *Science advances*, vol. 3, no. 9, p. e1700458, 2017.

[27] L. Lin, X. Peng, and Y. Zheng, "Reconfigurable opto-thermoelectric printing of colloidal particles," *Chemical Communications*, vol. 53, no. 53, pp. 7357–7360, 2017.

[28] H. Ding, P. S. Kollipara, L. Lin, and Y. Zheng, "Atomistic modeling and rational design of optothermal tweezers for targeted applications," *Nano Research*, vol. 14, no. 1, pp. 295–303, 2021.

[29] C. Min and X. Xie, "Graphene-based opt-thermoelectric nanotweezers," in *Advanced Optical Imaging Technologies III*, vol. 11549, p. 115490X, International Society for Optics and Photonics, 2020.

[30] R. S. Sheng, L. Zhu, and M. D. Morris, "Sedimentation classification of silver colloids for surface-enhanced raman scattering," *Analytical Chemistry*, vol. 58, no. 6, pp. 1116–1119, 1986.

[31] G. Schmid, "Large clusters and colloids. metals in the embryonic state," *Chemical reviews*, vol. 92, no. 8, pp. 1709–1727, 1992.

[32] G. Tripathi and M. Clements, "Adsorption of 2-mercaptopyrimidine on silver nanoparticles in water," *The Journal of Physical Chemistry B*, vol. 107, no. 40, pp. 11125–11132, 2003.

[33] P. Lee and D. Meisel, "Adsorption and surface-enhanced raman of dyes on silver and gold sols," *The Journal of Physical Chemistry*, vol. 86, no. 17, pp. 3391–3395, 1982.

[34] E. C. Le Ru and P. G. Etchegoin, "Chapter 7 - metallic colloids and other sers substrates," in *Principles of Surface-Enhanced Raman Spectroscopy* (E. C. Le Ru and P. G. Etchegoin, eds.), pp. 367–413, Amsterdam: Elsevier, 2009.

[35] Z. S. Pillai and P. V. Kamat, "What factors control the size and shape of silver nanoparticles in the citrate ion reduction method?," *The Journal of Physical Chemistry B*, vol. 108, no. 3, pp. 945–951, 2004.

[36] G. P. Kumar, S. Shruthi, B. Vibha, B. A. Reddy, T. K. Kundu, and C. Narayana, "Hot spots in ag core- au shell nanoparticles potent for surface-enhanced raman scattering studies of biomolecules," *The Journal of Physical Chemistry C*, vol. 111, no. 11, pp. 4388–4392, 2007.

[37] Y. Cui, B. Ren, J.-L. Yao, R.-A. Gu, and Z.-Q. Tian, "Synthesis of agcoreaushell bimetallic nanoparticles for immunoassay based on surface-enhanced raman spectroscopy," *The Journal of Physical Chemistry B*, vol. 110, no. 9, pp. 4002–4006, 2006.

[38] C. Kan, X. Zhu, and G. Wang, "Single-crystalline gold microplates: synthesis, characterization, and thermal stability," *The Journal of Physical Chemistry B*, vol. 110, no. 10, pp. 4651–4656, 2006.

[39] C. T. Rueden, J. Schindelin, M. C. Hiner, B. E. DeZonia, A. E. Walter, E. T. Arena, and K. W. Eliceiri, "Imagej2: Imagej for the next generation of scientific image data," *BMC bioinformatics*, vol. 18, no. 1, p. 529, 2017.

[40] D. Allan, T. Caswell, N. C. Keim, and C. M. van der Wel, "Trackpy v0.4.1,"

[41] P. P. Patra, R. Chikkaraddy, R. P. Tripathi, A. Dasgupta, and G. P. Kumar, "Plasmofluidic single-molecule surface-enhanced raman scattering from dynamic assembly of plasmonic nanoparticles," *Nature communications*, vol. 5, no. 1, pp. 1–8, 2014.

[42] W. Li, I. Kanyo, C.-H. Kuo, S. Thanneeru, and J. He, "ph-programmable self-assembly of plasmonic nanoparticles: hydrophobic interaction versus electrostatic repulsion," *Nanoscale*, vol. 7, no. 3, pp. 956–964, 2015.

[43] P. Taladriz-Blanco, N. J. Buurma, L. Rodríguez-Lorenzo, J. Pérez-Juste, L. M. Liz-Marzán, and P. Hervés, "Reversible assembly of metal nanoparticles induced by penicillamine. dynamic formation of sers hot spots," *Journal of Materials Chemistry*, vol. 21, no. 42, pp. 16880–16887, 2011.

[44] B. Su, J.-P. Abid, D. J. Fermín, H. H. Girault, H. Hoffmannová, P. Krtil, and Z. Samec, "Reversible voltage-induced assembly of au nanoparticles at liquid— liquid interfaces," *Journal of the American Chemical Society*, vol. 126, no. 3, pp. 915–919, 2004.

[45] S. Si, M. Raula, T. K. Paira, and T. K. Mandal, "Reversible self-assembly of carboxylated peptide-functionalized gold nanoparticles driven by metal-ion coordination," *ChemPhysChem*, vol. 9, no. 11, pp. 1578–1584, 2008.